



Probing Dark Energy with Supernovae: Exploiting Complementarity with the Cosmic Microwave Background

Joshua A. Frieman,^{1,2} Dragan Huterer,³ Eric V. Linder,⁴ and Michael S. Turner^{1,2,5}

¹*Department of Astronomy & Astrophysics, Center for Cosmological Physics,
The University of Chicago, Chicago, IL 60637-1433*

²*NASA/Fermilab Astrophysics Center Fermi National Accelerator Laboratory, Batavia, IL 60510-0500*

³*Department of Physics Case Western Reserve University, Cleveland, OH 44106-7079*

⁴*Physics Division, Lawrence Berkeley National Laboratory, Berkeley, CA 94720*

⁵*Department of Physics, Enrico Fermi Institute,
The University of Chicago, Chicago, IL 60637-1433*

A primary goal for cosmology and particle physics over the coming decade will be to unravel the nature of the dark energy that drives the accelerated expansion of the Universe. In particular, determination of the equation-of-state of dark energy, $w \equiv p/\rho$, and its time variation, dw/dz , will be critical for developing theoretical understanding of the new physics behind this phenomenon. Type Ia supernovae (SNe) and cosmic microwave background (CMB) anisotropy are each sensitive to the dark energy equation-of-state. SNe alone can determine $w(z)$ with some precision, while CMB anisotropy alone cannot because of a strong degeneracy between the matter density Ω_M and w . However, we show that the Planck CMB mission can significantly improve the power of a deep SNe survey to probe w and especially dw/dz . Because CMB constraints are nearly orthogonal to SNe constraints in the Ω_M - w plane, for constraining $w(z)$ Planck is more useful than precise determination of Ω_M . We discuss how the CMB/SNe complementarity impacts strategies for the redshift distribution of a supernova survey to determine $w(z)$ and conclude that a well-designed sample should include a substantial number of supernovae out to redshifts $z \sim 2$.

I. INTRODUCTION

Recent observations of Type Ia supernovae (SNe) have provided direct evidence that the Universe is accelerating [1, 2], indicating the existence of a nearly uniform dark-energy component with negative effective pressure, $w \equiv p/\rho < -1/3$. Further evidence for dark energy comes from recent cosmic microwave background (CMB) anisotropy measurements pointing to a spatially flat, critical density Universe, with $\Omega_0 = 1$, combined with a number of indications that the matter density $\Omega_M \simeq 0.3$ [3]; the ‘missing energy’ must also have sufficiently negative pressure in order to allow time for large-scale structure to form [4]. Together, these two lines of evidence indicate that dark energy composes 70% of the energy density of the Universe and has equation-of-state parameter $w < -(0.5 - 0.6)$ [5]. Determining the nature of dark energy, in particular its equation-of-state, is a critical challenge for physics and cosmology.

At present, particle physics theory provides little to no guidance about the nature of dark energy. A cosmological constant—the energy associated with the vacuum—is the simplest but not the only possibility; in this case, $w = -1$ and is time independent, and the dark energy density is spatially constant. Unfortunately, theory has yet to provide a consistent description of the vacuum: the energy density of the vacuum, at most 10^{-10} eV^4 , is at least 57

orders of magnitude smaller than what one expects from particle physics—the cosmological constant problem [6]. In recent years, a number of other dark energy models have been explored, from slowly rolling, ultra-light scalar fields to frustrated topological defects [7]. These models predict that $w \neq -1$, that w may evolve in time, and that there may be small spatial variations in the dark energy density (of less than a part in 10^5 on scales $\sim H_0^{-1}$ [8]). In all models proposed thus far dark energy can be characterized by its equation-of-state w . Measuring the present value of w and its time variation will provide crucial clues to the underlying physics of dark energy.

As far as we know, dark energy can only be probed directly by cosmological measurements, although it is possible that laboratory experiments could detect other physical effects associated with dark energy, e.g., a new long-range force arising from an ultra-light scalar field [9]. Dark energy affects the expansion rate of the Universe and thereby influences cosmological observables such as the distance vs. redshift, the linear growth of density perturbations, and the cosmological volume element (see, e.g., [10]). Standard candles such as Type Ia supernovae offer a direct means of mapping out distance vs. redshift, while the CMB anisotropy can be used to accurately determine the distance to one redshift, the last scattering epoch ($z_{LS} \simeq 1100$). Because they measure distances at such different redshifts, the SNe and CMB measurements

have complementary degeneracies in the Ω_M - w plane, as has been emphasized previously [10]. More recently, Spergel & Starkman [11] have suggested that this complementarity argues for using supernovae at relatively low redshift, $z \sim 0.4$, to most efficiently probe dark energy. In so doing, they used a highly simplified model which did not consider a spread of SNe in redshift, systematic error, possible evolution of w , or the finite precision with which planned CMB missions can actually constrain Ω_M and w .

By including these “real-world” effects, this paper clarifies the complementarity of the CMB and SNe and explores strategies for best utilizing it in SNe surveys to probe the properties of dark energy. We show that dark energy-motivated supernova surveys should target SNe over a broad range of redshifts out to $z \sim 2$, and that CMB/SNe complementarity in fact strengthens the case for deep SNe surveys.

II. HOW SUPERNOVAE AND THE CMB PROBE DARK ENERGY

Supernovae and the CMB anisotropy probe dark energy in different ways and at different epochs. However, both do so through the effect of dark energy on the co-moving distance vs. redshift relation, $r(z)$. For a spatially flat Universe and constant w :

$$H_0 r(z) = \int_0^z \frac{dz}{H(z)/H_0} \quad (1)$$

$$(H/H_0)^2 = \Omega_M(1+z)^3 + (1-\Omega_M)(1+z)^{3(1+w)}$$

where Ω_M is the present fraction of the energy density contributed by non-relativistic matter. This relation is easily generalized to non-constant w and a curved Universe [10]; for notational simplicity we write this and succeeding formulae in terms of constant w , though we generalize them to the evolving case in our analysis. It is because $H_0 r(z)$ depends upon only two quantities, Ω_M and w , that prior information about Ω_M (or two independent combinations of Ω_M and w) has such potential to improve the efficacy of a cosmological probe of dark energy based upon $H_0 r(z)$.

CMB experiments can determine the positions and heights of the acoustic peaks in the temperature anisotropy angular power spectrum to high accuracy. The positions of the acoustic peaks in angular multipole space depend upon the physical baryon and matter densities $\Omega_B h^2$ and $\Omega_M h^2$, on Ω_M , w , and to a lesser extent other cosmological parameters (e.g., [10, 14]). Anisotropy measurements from the Planck [15] mission, planned for launch later in the decade, should determine the positions of the peaks to better than 0.1%; the heights of the peaks will determine $\Omega_M h^2$ and $\Omega_B h^2$ (and other cosmological parameters) to roughly percent precision [16]. Together, these measurements should constrain a combination of Ω_M and w alone (e.g., [10, 11]) to about

10% precision. In particular, in the vicinity of the fiducial values $w_0 = -1$ and $\Omega_{M0} = 0.3$, the combination

$$\begin{aligned} \mathcal{D} &\equiv \Omega_M - 0.94 \Omega_{M0}(w - w_0) \\ &\approx \Omega_M - 0.28(1 + w) = 0.3 \end{aligned} \quad (2)$$

will be determined to about $\sigma_{\mathcal{D}} \simeq \pm 0.03(\Omega_{M0}/0.3)$ (this result follows directly from Eq. 18 of Ref. [10] by setting $\Delta l/l = \Delta\Omega_0/\Omega_0 = 0$). The resulting 68% CL error ellipse in the Ω_M - w plane predicted for Planck is shown in Fig. 1. Polarization information could in principle improve the precision with which \mathcal{D} is determined by about 50% [17], absent problems with foregrounds or the polarization measurements themselves.

The MAP CMB mission [18] currently underway should determine \mathcal{D} to a precision that is about 10 times worse than Planck, assuming temperature anisotropy information alone. This constraint is too weak to usefully complement the SNe measurements. However, if MAP polarization measurements are successful, this constraint could be improved by about a factor of two [17]; we discuss the potential impact of MAP further in Sec. IV A 3.

As an aside, we note that the physical baryon and matter densities do not directly impact the determination of the properties of dark energy. Rather, together with other cosmological measurements, they can be used to determine Ω_M . In the following Sections we illustrate how independent knowledge of Ω_M can improve the determination of w .

Measurements of the energy fluxes and redshifts of Type Ia supernovae provide an estimate of the luminosity distance as a function of redshift, $d_L \equiv (1+z)r(z)$. As an example of a supernova survey, the Supernova/Acceleration Probe (SNAP) [19] is a proposed space-based telescope to observe ~ 3000 SNe Ia out to redshift $z \sim 1.7$, specifically designed to probe dark energy. To illustrate the essential principles for such a survey, though not all the details, we make the simplifying assumption that SNe Ia are nearly standard candles (after correction for the observed correlation between light-curve decline rate and peak luminosity [20]). With this assumption, the mean peak energy flux from a supernova at redshift z is:

$$\begin{aligned} F(z) &= \frac{\mathcal{C}10^{-0.4M}}{4\pi d_L^2} = \frac{(10^{10}\mathcal{C}/4\pi)10^{-0.4\mathcal{M}}}{H_0^2 d_L^2} = \\ &= \frac{(10^{10}\mathcal{C}/4\pi)10^{-0.4\mathcal{M}}}{(1+z)^2 \left[\int_0^z \frac{dz}{\sqrt{\Omega_M(1+z)^3 + (1-\Omega_M)(1+z)^{3(1+w)}}} \right]^2} \end{aligned} \quad (3)$$

where $\mathcal{C} = 3.02 \times 10^{35}$ erg sec $^{-1}$ is an unimportant constant, M is the mean absolute peak magnitude of a Type Ia supernova, and $\mathcal{M} = M - 5 \log(H_0) + 25$, with distances measured in Mpc.

It is important to note several things from Eq. (3). First the energy flux at fixed $H_0 d_L$ depends only upon

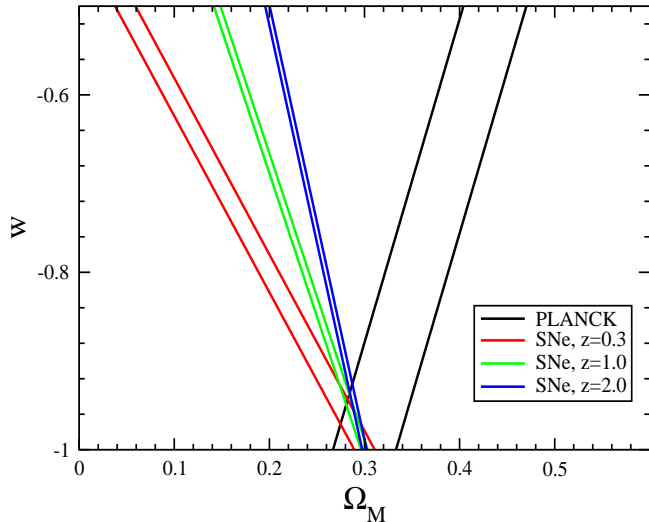


FIG. 1: 68% CL “error ellipses” in the Ω_M - w plane for 3000 SNe all at a single redshift $z = 0.3, 1.0$, or 2.0 , and for the Planck CMB anisotropy measurement (without polarization), assuming a fiducial model with $\Omega_{M0} = 0.3$ and $w_0 = -1$. Because observations at a single redshift cannot break the parameter degeneracies, the ellipses do not close. As expected, the CMB constraint lies along $\Omega_M \simeq 0.3 + 0.28(1 + w)$. At higher z , the SNe ellipses become narrower but less orthogonal (complementary) to the CMB ellipse. Note, a matter-density prior corresponds to a vertical stripe, which is less orthogonal to the SNe ellipses than the CMB ellipse. This is the basic reason why a CMB prior is more effective than a matter-density prior.

the combination \mathcal{M} and not upon M and H_0 separately. Thus, the cosmological parameters Ω_M and w can be determined by measuring ratios of fluxes at different redshifts, which are independent of \mathcal{M} , and so \mathcal{M} is sometimes referred to as a nuisance parameter and can be easily marginalized over. Second, since $H_0 d_L \rightarrow z$ for $z \rightarrow 0$, low-redshift supernovae can be used to determine \mathcal{M} ,

$$z^2 F(z) \rightarrow (10^{10} \mathcal{C}/4\pi) 10^{-0.4\mathcal{M}} \text{ as } z \rightarrow 0. \quad (4)$$

For example, a sample of 300 low-redshift supernovae (e.g., as will be targeted by the Nearby SN Factory [21]) could be used to pin down \mathcal{M} to a precision of $\pm(0.01 - 0.02)$. Finally, an absolute calibration of nearby SNe Ia luminosities by another reliable distance indicator (e.g., using Cepheid variables to determine distances to galaxies that host SNe Ia [22]) can determine M ; together, M and \mathcal{M} then fix the Hubble constant, but we emphasize that this is not needed to probe dark energy.

For a survey of SNe Ia, the likelihood function for the three parameters the supernova energy flux depends

upon is given by

$$\mathcal{L}_{\text{SNe}}(\Omega_M, w, \mathcal{M}) \propto \prod_i \exp\left(-\frac{[F_i - F(z_i)]^2}{2\sigma_i^2}\right) \quad (5)$$

where z_i are the redshifts of the supernovae, F_i are their measured fluxes, and σ_i are their measurement uncertainties (which also includes any random intrinsic spread in peak SNe Ia luminosities).

Unlike the CMB, which probes the angular diameter distance at a single, fixed redshift z_{LS} , the efficacy of SNe for determining w depends upon the redshift distribution of the supernovae. As a first example, Fig. 1 shows how well 3000 supernovae at a single redshift could constrain Ω_M and w , assuming a random flux error of 0.15 mag per supernova. Because the sensitivity of the comoving distance $r(z)$ to the dark energy equation-of-state (e.g., as measured by dr/dw) increases with redshift, the ellipse shrinks for SNe at higher redshift [10].

While Fig. 1 displays important trends, we note that a realistic survey would not target SNe all at one redshift. Such a delta-function redshift distribution is very much less than optimal for constraining w (as we show in Sec. IV A) and would be very inefficient, since large numbers of discovered SNe would have to be discarded. More importantly, a broad distribution of SNe redshifts is crucial for addressing systematic/evolutionary trends in the SNe population, which must be under control if SNe (or anything else) are to be valid probes of dark energy.

In addition, there is much more to studying dark energy than determining the average value of w in the most efficient manner. Constraining the time variation of the equation-of-state is critical for understanding the nature of dark energy. The CMB has no sensitivity to evolution of w ; SNe can probe time variation of w , and a broad distribution of SNe redshifts (out to $z \sim 2$) is required to achieve it, as we show below. In Sec. IV we discuss strategies for the distribution of SNe redshifts and results for some plausible examples. Finally, determining cosmological parameters (here Ω_M and w) by two very different techniques has the virtue of providing consistency checks on the framework of dark energy as well as the Friedmann-Robertson-Walker cosmology [12, 13].

III. CMB/SNE COMPLEMENTARITY

Some trends in the CMB/SNe complementarity are illustrated in Fig. 1. For the fiducial model ($w_0 = -1$, $\Omega_{M0} = 0.3$), the Planck error ellipse in the Ω_M - w plane is approximately oriented along the line $\Omega_M \simeq 0.3 + 0.28(1 + w)$, as indicated by Eq. (2). By contrast, the error ellipse for 3000 SNe at fixed redshift has negative slope in this plane; with increasing redshift it rotates toward $\Omega_M = \text{const}$, and its width narrows. The reason for the rotation is simple: at high redshift, matter becomes more dynamically important than dark energy, and the SNe are therefore probing the matter density.

While the width of the SNe ellipse shrinks with increasing redshift, it becomes less complementary with the CMB ellipse. Fig. 1 also makes it clear why CMB anisotropy is more complementary than the matter density information: the matter density prior, which corresponds to a vertical stripe, is less orthogonal to the SNe ellipse.

To be quantitative, it is useful to write down the joint likelihood function:

$$\mathcal{L}_{\text{joint}} = \mathcal{L}_{\text{SNe}} \times \mathcal{L}_{\text{CMB}} \times \mathcal{L}_{\text{other}}. \quad (6)$$

The CMB likelihood function can be approximated as

$$\mathcal{L}_{\text{CMB}} = \mathcal{L}_{\text{CMB},0}(\Omega_M, w) \times \exp \left[-\frac{(\rho_B - \rho_{B0})^2}{2\sigma_{\rho_B}^2} \right] \times \exp \left[-\frac{(\rho_M - \rho_{M0})^2}{2\sigma_{\rho_M}^2} \right] \quad (7)$$

where

$$\mathcal{L}_{\text{CMB},0} \propto \exp \left[-\frac{(\mathcal{D} - \mathcal{D}_0)^2}{2\sigma_{\mathcal{D}}^2} \right], \quad (8)$$

$\mathcal{D} = \Omega_M - 0.28(1+w)$, $\mathcal{D}_0 \simeq 0.3$ is the fiducial value of \mathcal{D} , $\sigma_{\mathcal{D}} \simeq 0.1\mathcal{D}_0$ is the projected accuracy for Planck¹, $\rho_B \equiv 1.88\Omega_B h^2 \times 10^{-29} \text{ g cm}^{-3}$, $\rho_M \equiv 1.88\Omega_M h^2 \times 10^{-29} \text{ g cm}^{-3}$, ρ_{B0} is the fiducial value of the baryon density, and ρ_{M0} is the fiducial value of the matter density.

As noted in Sec. II, the CMB determination of the baryon and matter densities is not directly useful for constraining dark energy: when the joint likelihood function is marginalized over the matter and baryon densities to obtain the one-dimensional probability distribution for w , the integrations over $\Omega_B h^2$ and $\Omega_M h^2$ are trivial. On the other hand, if we can obtain information about M (from non-SNe distance measurements) and \mathcal{M} (from low-redshift SNe) and thereby (or otherwise) constrain H_0 , then the CMB determination of $\Omega_M h^2$ constrains Ω_M as well, which would directly impact the joint determination of w . Of course, any other external determination of Ω_M would have the same effect; later, we will discuss how various Ω_M priors affect the determination of w .

Assuming no information about M (or equivalently H_0), the joint likelihood function becomes

$$\mathcal{L}_{\text{joint}}(\Omega_M, w) = \mathcal{L}_{\text{CMB},0} \times \mathcal{L}_{\text{SNe}} \quad (9)$$

From this function, we obtain one-dimensional probability distributions for w by marginalizing over Ω_M . As a first case, we again assume a baseline sample of 3000 SNe all at one redshift, with a random flux error of 0.15 mag per supernova. In Fig. 2, we show the effect of including CMB or Ω_M information in the determination of the

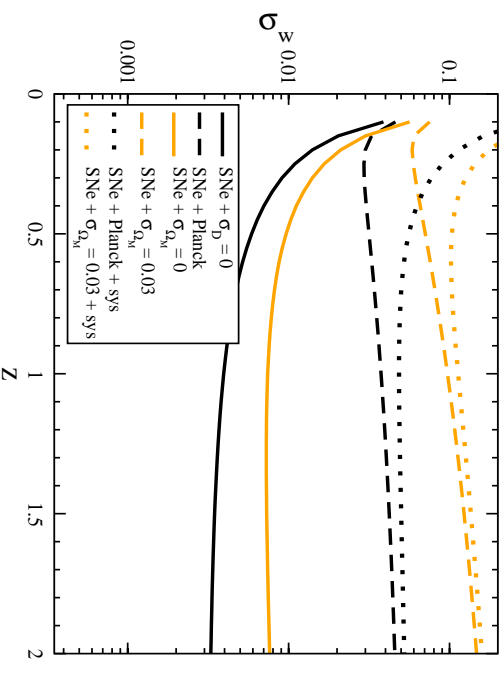


FIG. 2: The predicted $1\text{-}\sigma$ uncertainty in the equation-of-state parameter w for 3000 SNe at a single redshift z , with matter density and CMB priors as indicated (and the same fiducial model as in Fig. 1). The dotted curve in each case includes the effect of a 0.02 mag irreducible systematic error in measuring the energy flux. The progression from “solid to dashed to dotted” goes from “ideal to realistic.”

dark energy equation-of-state, assuming $w = \text{const.}$ If the CMB measurement of \mathcal{D} is assumed to be “perfect” ($\sigma_{\mathcal{D}} = 0$) as was done in Ref. [11], the predicted σ_w drops significantly with increasing redshift and continues to do so out to $z \approx 1.5$. The effect of a “perfect” matter density prior ($\sigma_{\rho_M} = 0$) is similar. This qualitative behavior can be understood by referring to Fig. 1 and considering the intersection of the CMB line (now an infinitely thin ellipse) with the SNe ellipses or of a vertical line (fixed Ω_M) with the SNe ellipses. The decreasing width of the SNe ellipses wins out over the decreasing complementarity at higher redshift.

The qualitative behavior changes, however, when finite precision for the CMB and matter density measurements is taken into account; as examples, for the CMB we use the projected Planck accuracy discussed above, and for the matter density we assume $\sigma_{\rho_M} = 0.03$. Not only is the uncertainty σ_w larger in these cases, but it now reaches a minimum at $z \sim 0.2$ and rises slightly at higher redshift. For finite widths of the matter density or CMB priors, the decreasing complementarity now wins out over the decreasing width of the SNe ellipse with increasing redshift.

Thus far, we have not allowed for systematic error in measuring the supernova flux at a given redshift. This means that by measuring a large number of supernovae at a given redshift, the flux and thereby $r(z)$ can be determined to arbitrarily high accuracy. In reality, the

¹Note that this is merely illustrative. In fact we treat \mathcal{D} by the exact expression for the distance to the last scattering surface, i.e., Eq. (1) generalized to evolving $w(z)$.

presence of residual systematic uncertainty is likely to impose a floor to improvement. As a simple model for irreducible systematic error in the SNe measurements, we assume the flux error in a specified redshift interval is given by $\sqrt{(0.02)^2 + (0.15)^2/N_i}$ mag, where 0.15 mag is the assumed statistical error per SN, 0.02 mag is the irreducible error,² and N_i is the number of supernovae observed in that redshift interval. This model penalizes observing large numbers of SNe at the same redshift since the irreducible error adds to the Poisson error: one reaches diminishing returns for $N_i \sim 100$, at which point the error is only $\sim 20\%$ larger than its asymptotic value. While this model is certainly simplistic, it captures in a straightforward way the essential point: increasing the number of SNe cannot decrease the measured error in $H_0 r(z_i)$ to arbitrarily small values [23].

Figure 2 illustrates the effect of systematic error. At redshifts less than about $z \sim 0.5$, systematic error increases σ_w significantly: without the irreducible flux error, the estimate for σ_w was optimistically small because the flux error was allowed to decrease to a tiny value (~ 0.003 mag). With systematic flux error included, the predicted error in w from a combined Planck CMB measurement and a hypothetical sample of 3000 SNe (all at redshift z) flattens at $z \sim 1$, with an asymptotic amplitude $\sigma_w \simeq 0.05$.

As noted in Sec. II, realistic survey would not target supernovae all at a single redshift, as assumed up to now. Moreover, since the orientation of the SN error ellipse in the Ω_M - w plane rotates with z (see Fig. 1), a spread of SNe redshifts helps break the degeneracy between Ω_M and w . In the next Section, we consider more realistic strategies for the supernova redshift distribution to optimally probe dark energy.

IV. STRATEGIES FOR CMB/SNE COMPLEMENTARITY

A Optimal

The issue of optimal strategies for determining dark energy properties using SNe in a realistic experiment has been addressed in Refs. [10, 24]. Here, we extend these results to incorporate CMB anisotropy and other measurements.

²In practice, the level of the residual systematic error depends on survey design, e.g., telescope aperture and stability, wavelength coverage, observing cadence, point spread function, seeing, sky background, etc. The systematic error quoted here is based on the fact that SNAP is specifically designed to achieve 0.02 mag systematic error in redshift bins of width $\Delta z = 0.1$.

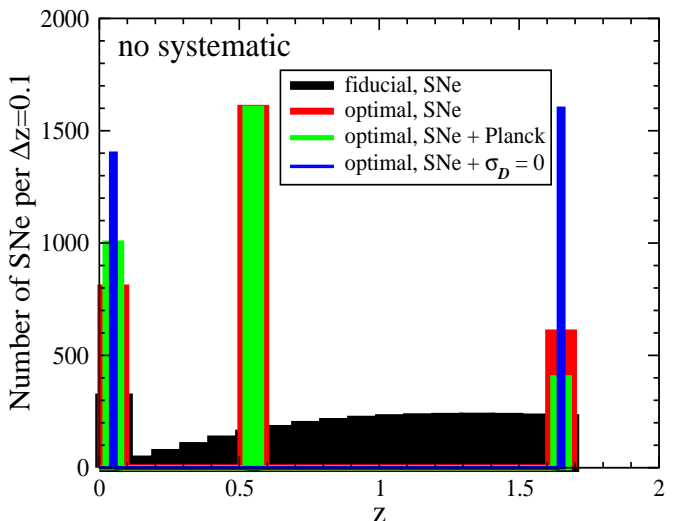


FIG. 3: Optimal redshift distributions in bins of width $\Delta z = 0.1$ for determining w from SNe alone (red) and with CMB information added (green and blue). All cases assume $z_{\max} = 1.7$ and no systematic error. The perfect CMB prior (blue, $\sigma_{\mathcal{D}} = 0$) is a “strong” prior: the optimal distribution comprises two delta functions; the Planck CMB prior (green) is not “strong”, as three delta functions remain. For comparison, the black histogram shows a “fiducial” SNAP + SN Factory redshift distribution with 2812+300 SNe.

1 No systematic error

The optimization problem can be stated as follows: we have three cosmological parameters (\mathcal{M} , Ω_M , and w ; later we will add a fourth, dw/dz); we have “prior information” (from the CMB anisotropy and/or an independent determination of Ω_M); and we wish to determine the redshift distribution of the SNe which minimizes the error on w , with the constraint that they are confined to the interval $[0, z_{\max}]$. For now, we assume that the total number of observed SNe is held fixed, and we do not include systematic error in the SNe measurements. Later we will relax both of these assumptions.

Huterer & Turner [10] showed that for the N -parameter problem with no priors, the optimal redshift distribution comprises N delta functions, with one at $z = 0$, one at z_{\max} , and the others in between. The amplitudes of the delta functions and their positions relative to z_{\max} vary little with the value of z_{\max} .³ Adding a “strong” prior on one, or a combination, of the three

³The optimization can be done with respect to the errors of the individual parameters or the determinant of the Fisher matrix (“area of error ellipse” for the two-parameter problem). The results in the two cases are similar. We will minimize σ_w unless otherwise

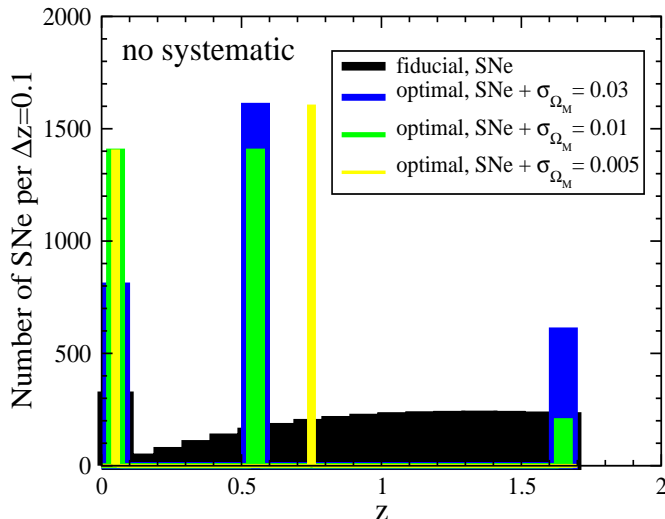


FIG. 4: Same as Fig. 3, except with matter density priors of $\sigma_{\Omega_M} = 0.03$ (blue), 0.01 (green), and 0.005 (yellow). The matter density prior is only “strong” for $\sigma_{\Omega_M} \leq 0.005$. For a strong matter-density prior, the delta function at z_{\max} disappears because the highest redshift SNe preferentially probe the matter density.

parameters reduces the number of delta functions by one, adding two “strong” priors reduces the number of delta functions by two, and so on. A “strong” prior is one that constrains one, or a combination, of the three parameters better than the SNe measurements alone would. In actuality, this is a continuous process, with the amplitude of one of the delta functions going to zero as the quality of the prior improves. Further, for smaller z_{\max} it is easier to have a “strong” prior, since the SNe constrain the parameters less well.

For illustration we consider a survey of about 3000 SNe with survey depth $z_{\max} = 1.7$. These choices are motivated by the proposed SNAP survey [19] and thus provide a useful benchmark (SNAP should obtain 3000 Type Ia SNe in about two years of observations). Figure 3 shows the optimal SNe redshift distribution with no CMB prior, a perfect CMB prior ($\sigma_{\mathcal{D}} = 0$), and the Planck prior (see Sec. III). For comparison, we also show one of the redshift distributions currently proposed for SNAP (2812 SNe in the redshift interval 0.1 – 1.7) combined with that for the Nearby SN Factory (300 SNe at $z < 0.1$). We see that a “perfect” CMB prior is a “strong” prior: the optimal SNe distribution in this case becomes two delta functions, one at $z = 0$ and one at $z = z_{\max}$. The Planck prior is not strong: in this case, three delta functions remain, at $z = 0, 0.5$, and 1.7. Figure 4 shows

noted.

the optimal SNe redshift distribution using Ω_M instead of CMB priors, with $\sigma_{\Omega_M} = 0.005, 0.01$, and 0.03. The Ω_M prior is only “strong” for $\sigma_{\Omega_M} \leq 0.005$.

In Figs. 3 and 4, the $z \sim 0$ peaks in the optimal distributions serve mainly to determine \mathcal{M} . Indeed, the Nearby SN Factory redshift distribution is strongly peaked at $z \approx 0.05$, in part for this reason.⁴ We could have simply imposed a prior on \mathcal{M} instead of including this portion of the redshift distribution.

Finally, it is important to consider how much improvement the optimal redshift distribution actually provides compared to a uniform distribution or the SNAP+SN Factory distribution: for the cases shown in Figs. 3 and 4, σ_w is typically 20% to 30% smaller for the optimal distribution.

2 Inclusion of systematic error and evolution of w

Now we consider the effect of systematic flux error on the optimal SNe redshift distribution. As before, we use the simple model of an irreducible flux error of 0.02 mag in each redshift interval of width $\Delta z = 0.1$. We should expect that this will broaden the optimal distribution, since it is more expedient to spread the remaining SNe to other redshift bins once the error in a given bin becomes comparable to the irreducible error. Figs. 5 and 6 show the optimal SNe redshift distributions, with and without CMB and Ω_M priors, in the presence of systematic errors. Figs. 5a and 6a show results for the $w = \text{const}$ case as before, while Figs. 5b and 6b allow for evolution of the equation-of-state, $w(z) = w_0 + w_1 z$, with $w_1 = dw/dz|_{z=0}$. Comparison of Figs. 5a and 6a with Figs. 3 and 4 shows that inclusion of systematic error indeed changes the optimal distribution significantly, broadening it to become more uniform.

For the case of constant w (Figs. 5a and 6a), the gain in performance for the optimal SNe distribution vs. a uniform or SNAP+SN Factory distribution is reduced to only 3–5% when systematic errors are included. We find that a number of qualitatively different redshift distributions yield essentially the same value of σ_w . In particular, in this case σ_w is relatively insensitive to z_{\max} : there exist distributions with no SNe at $z > 1$ which yield σ_w only 3% larger than the optimal value (see also Fig. 7 below).

The situation is markedly different if we allow for time variation in the equation-of-state. In Figs. 5b and 6b, we show the distributions that minimize σ_{w_1} (the results are almost identical if σ_{w_0} is minimized instead). In the presence of CMB or matter density priors, the optimal distributions now include larger numbers of SNe at high

⁴The SN Factory has another important purpose: the systematic study of Type Ia SNe to better establish their efficacy as standardizable candles.

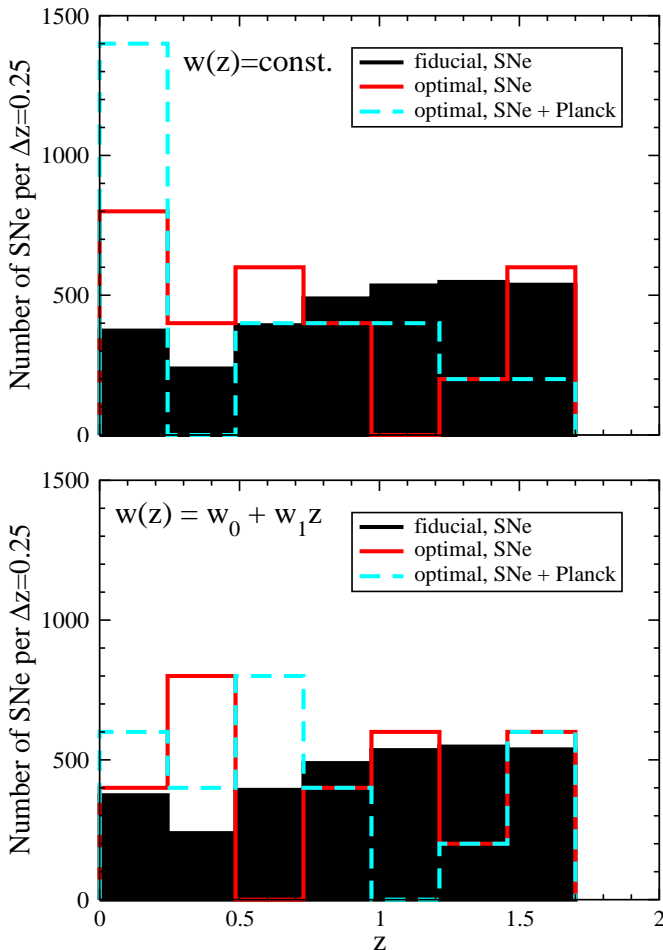


FIG. 5: Optimal redshift distributions for determining w by 3000 SNe measurements alone (red solid line) and for 3000 SNe + Planck CMB measurements (cyan dashed line), with $z_{\max} = 1.7$ and including systematic error. For comparison, the black histogram shows the fiducial SNAP + SN Factory redshift distribution. Bins of width $\Delta z \approx 0.25$ are used solely for numerical convenience. (a) Constant w ; (b) evolving equation-of-state, $w(z) = w_0 + w_1 z$. The optimal distributions are no longer sums of delta-functions when systematic error is taken into account.

redshift. Furthermore, SNe in the high-redshift range $1 < z < 1.7$ are crucial for precision constraints to w_1 , even in the presence of a strong prior. For example, as z_{\max} increases from 1 to 1.7, σ_{w_1} decreases by more than a factor of two, cf. Fig. 9.

3 Gains from complementarity

The preceding analysis shows that, for fixed z_{\max} , the error on w is only weakly dependent on the SNe red-

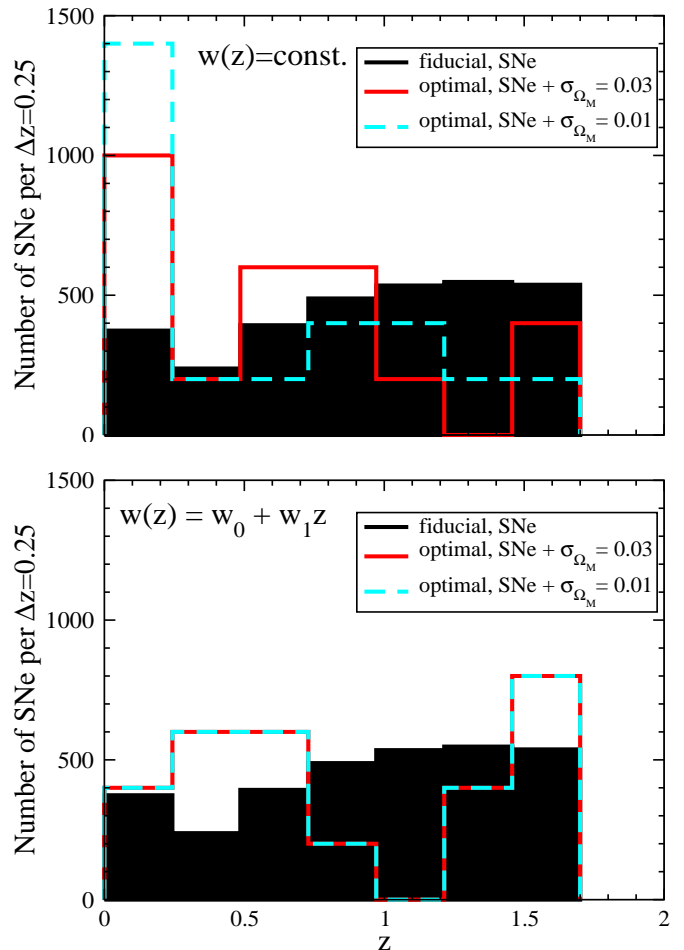


FIG. 6: Same as Fig. 5, except for matter-density priors.

shift distribution: in the presence of systematic error, distributions which are broadly spread over the range $0 < z < z_{\max}$ differ only slightly in their performance. Therefore the chief determinant of the error is z_{\max} itself, and we now address how the efficacy of SNe with complementary information depends on this maximum redshift. In Fig. 7, we show the effect of various CMB and matter density priors on the predicted value of σ_w vs. z_{\max} , assuming $w = \text{const}$, with systematic error modeled as before and assuming a scaled version of the SNAP + SN Factory distribution of redshifts.⁵ (As noted above, the optimal redshift distribution with the same value of z_{\max} would yield only slightly smaller σ_w .) Figure 7 also includes the error on w for the case of no CMB prior or

⁵When varying z_{\max} from its fiducial value of 1.7, we truncate the fiducial SNAP distribution at the new z_{\max} and scale it to preserve the total of 2812 SNe. The SN Factory distribution is then added unchanged – 300 SNe in the lowest redshift bin.

knowledge of the matter density (black curve).

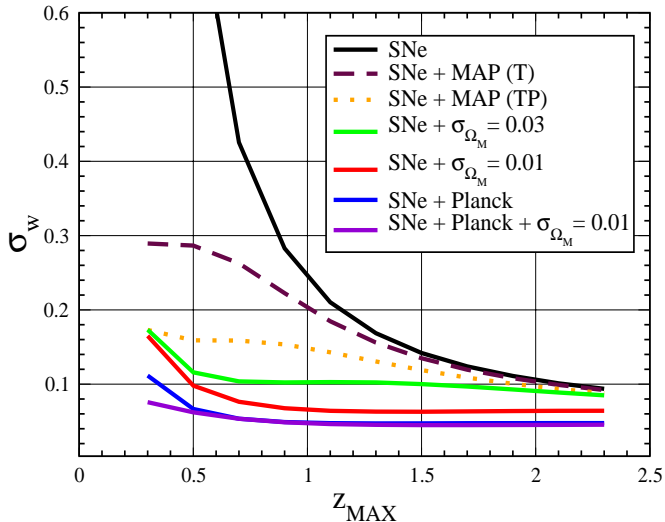


FIG. 7: The predicted σ_w vs. SNe survey depth for a combined set of experiments: (a) SNe only (black), (b) SNe + MAP (temperature only) (maroon dashed), (c) SNe + MAP (temperature and polarization) (orange dotted), (d) SNe + ($\sigma_{\Omega_M} = 0.03$) (green), (e) SNe + ($\sigma_{\Omega_M} = 0.01$) (red), (f) SNe + Planck (blue), and (g) SNe + Planck + ($\sigma_{\Omega_M} = 0.01$) (purple). In all cases, we assume the scaled SNAP + SN Factory redshift distribution and an irreducible systematic error in flux measurements of 0.02 mag in redshift bins $\Delta z = 0.1$.

The primary effect of incorporating additional information, from either the CMB or the matter density, is to dramatically decrease σ_w at redshifts less than one and thereby lessen the dependence of σ_w on z_{max} . With SNe only, σ_w decreases from 0.8 to 0.15 as z_{max} is increased from 0.5 to 1.5. With the Planck or matter density prior, σ_w decreases less rapidly and levels off at $z \sim 1$. Note that the Planck prior is more effective than either matter density prior shown. Even combining a $\sigma_{\Omega_M} = 0.01$ prior with Planck provides little improvement over the Planck prior alone. Although an independent determination of Ω_M to ± 0.03 can substantially improve the precision with which w can be determined if $z_{\text{max}} \leq 1.5$ [10], the Planck CMB prior by itself does better by a factor of two.

As mentioned at the end of Sec. II, time variation in the equation-of-state is generically expected and is a potentially important discriminator between dark energy models. Allowing for evolution, with $w(z) = w_0 + w_1 z$,⁶ there are now four parameters to determine: \mathcal{M} , Ω_M , w_0 , and w_1 . As Figs. 8 and 9 illustrate, without an additional

⁶As discussed in Ref. [10], the exact form chosen for the parameterization is not essential.

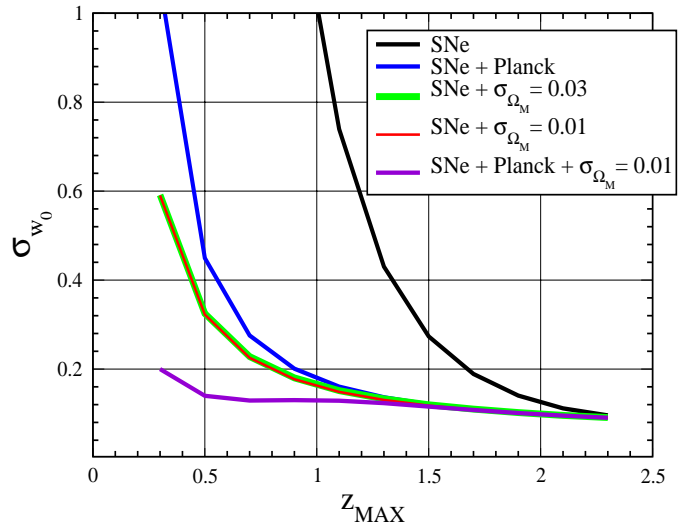


FIG. 8: Same as Fig. 7, but for w_0 , where $w(z) = w_0 + w_1 z$. The curves for SNe + MAP are not shown.

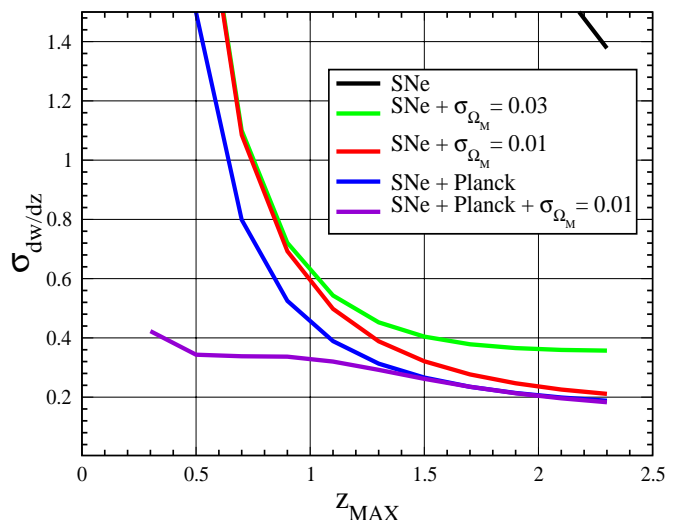


FIG. 9: Same as Fig. 7, but for $w_1 = (dw/dz)|_{z=0}$, where $w(z) = w_0 + w_1 z$. The curves for SNe + MAP are not shown.

prior, SNe have little leverage on w_0 and w_1 [10, 25]. An independent determination of the matter density to ± 0.03 – not much more stringent than already achieved: 0.04 [3] – would allow w_0 and w_1 to be determined to precision of about ± 0.1 and ± 0.35 for $z_{\text{max}} \sim 1.7$ [10]. The Planck prior is just as good as a $\sigma_{\Omega_M} = 0.03$ matter density prior for w_0 (if $z_{\text{max}} \geq 1$) and better for w_1 . Note that the improvement with survey depth in σ_{w_1} (and to a lesser extent σ_{w_0}) continues out to $z_{\text{max}} = 2$ in all cases. That is, even in the presence of complementary informa-

tion from the CMB or the matter density, a SNe survey aimed at detecting and constraining the evolution of the dark energy equation-of-state should extend out to high redshift, $z_{\max} \sim 1.5 - 2$.

Thus far, our discussion of CMB anisotropy has been confined to the Planck mission. It is also worth considering what can be learned from the ongoing MAP experiment. As noted in Sec. II, with temperature anisotropy measurements alone, MAP can determine \mathcal{D} about 10 times less accurately than Planck, $\sigma_{\mathcal{D}} \simeq 0.3$. In this case, MAP provides a far less useful prior than the matter density prior $\sigma_{\Omega_M} = 0.03$ (about a factor of two worse for σ_w), cf. Fig. 7. Even if MAP can achieve its full polarization capability (a factor of two improvement in $\sigma_{\mathcal{D}}$ [17]), a MAP prior is still not as good as the matter density prior $\sigma_{\Omega_M} = 0.03$. Moreover, mapping the polarization anisotropy on large angular scales — where it helps determine w indirectly, by imposing an upper limit to the ionization optical depth τ — will be difficult in the presence of polarized synchrotron radiation from the Galaxy. Finally, we mention that while polarization measurements also have the potential to improve the Planck determination of \mathcal{D} (by about 50%), this only improves the joint SNe/CMB determination of w by about 15%. The reason is simple: it is the width of the SNe error ellipse that controls σ_w .

B Resource limited

In the analysis so far, we have assumed a fixed total number of observed supernovae, $N_{SN} = 3112$. However, the resources required to discover and follow up a supernova depend in general upon its redshift. Thus, an important but more complicated problem involves the optimization of the determination of dark energy parameters with fixed total resources. Actually determining what these fixed resources are (e.g., discovery time, follow-up time, spectroscopy time) and how much each supernova ‘costs’ is beyond the scope of this paper (relevant ongoing studies can be found at [19]). We note that these costs will depend in detail upon a variety of technical factors: telescope aperture, pixel size and number, CCD quantum efficiency, sky brightness, atmospheric seeing (for ground-based observations), required signal to noise, etc.

As a highly simplified model, let the normalized cost of each supernova observed at redshift z be $(1+z)^m$, so that the total cost of a survey that follows up N supernovae is $\sum_{i=1}^N (1+z_i)^m$. The problem is to find the optimal SNe redshift distribution for fixed total resources (total cost) R . For SNAP, the observing time cost for spectroscopy or photometry per supernova is estimated to scale as $(1+z)^6$ for fixed signal to noise [19]. In the case of wide field, multiplexing photometry that SNAP is designed for, simultaneously discovering and following up supernovae by repeatedly sweeping the same field could

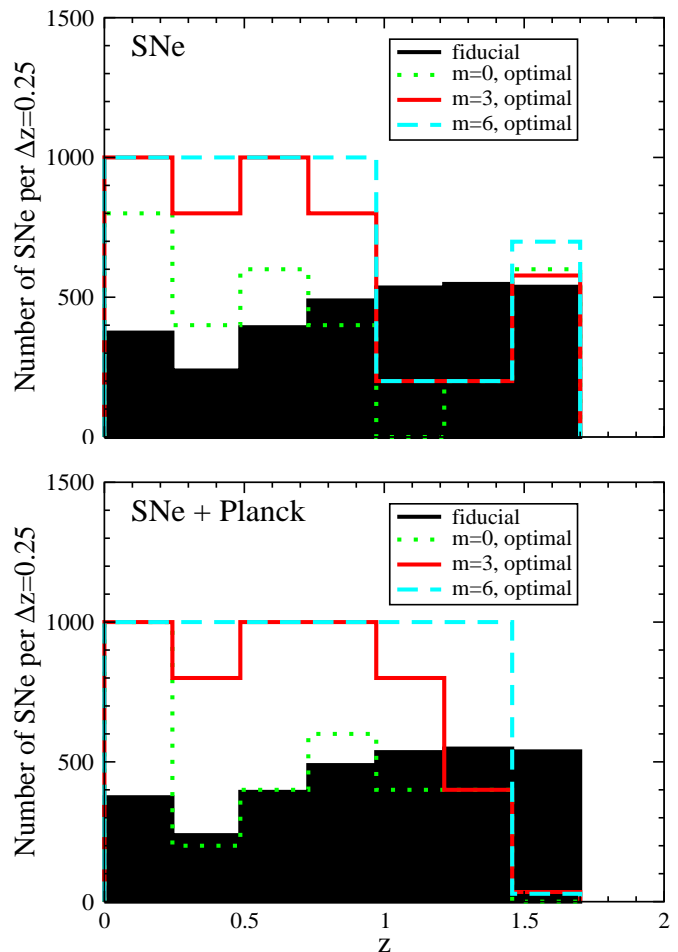


FIG. 10: The resource-optimized redshift distributions for determining (constant) w by (a) SNe measurements alone and (b) SNe + Planck, including systematic errors, assuming the cost per supernova scales as $(1+z)^m$, for $m = 0, 3, 6$. The fiducial SNAP + SN Factory distribution is shown for comparison.

reduce this by a large factor. To span the plausible range of cost functions, we show results for $m = 0, 3, \text{ and } 6$.

To fix the total resources R , we assume that there are sufficient resources to carry out a survey of 3112 SNe with the fiducial SNAP + SN Factory redshift distribution shown, e.g., in Fig. 3. That is, for a given value of m , we fix R by computing the total cost of the fiducial SNAP + SN Factory redshift distribution. Then we find the SN redshift distribution that minimizes σ_w within the resource constraint, i.e., for the same value of R . If we place no upper bound on the number of SNe per redshift bin, the number of SNe at low redshifts would be driven to huge values as m is increased. Clearly a distribution with many thousands of SNe in any redshift bin is not experimentally realistic, and the systematic error makes this an unwise choice: the gains in terms of reduced σ_w

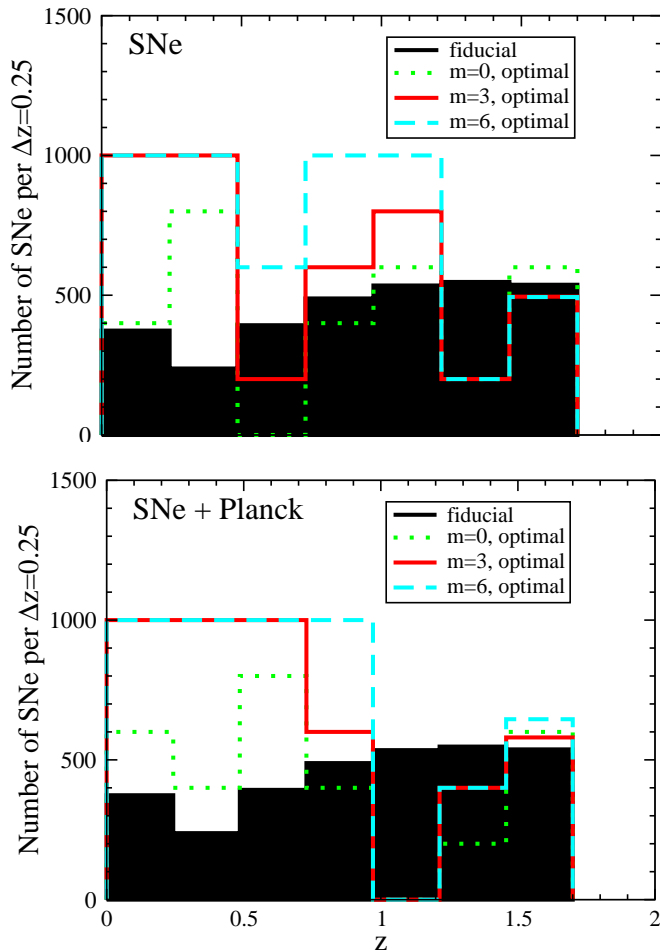


FIG. 11: Same as Fig. 10, but with $w(z) = w_0 + w_1 z$.

are negligible once the number of SNe per bin goes much above 100. We therefore impose the further constraint that the number of SNe per redshift bin of width 0.25 not exceed (a very generous) 1000.

The results for $m = 0, 3$, and 6 are shown in Figs. 10 and 11, again for $z_{\max} = 1.7$, the same model for irreducible systematic error as above, and either no prior from the CMB (Figs. 10a, 11a) or the Planck prior (Figs. 10b, 11b). In Fig. 10, we assume constant w , while in Fig. 11 w can evolve. We note that the performance of the optimal distribution in minimizing σ_w (or σ_{w_1}) is only 2 to 10% better than the SNAP + SN Factory distribution in all cases.

Consider first the constant w case. Figure 10 shows that, as m increases, SNe start filling up the lower redshift bins to the maximum allowed number; this continues until the resource limit is reached. While this is strictly true for the Planck prior, with no prior a significant fraction of SNe remain in the highest redshift bin. This behavior can be understood simply: without any priors, the high redshift SNe are crucial for breaking the

degeneracy between Ω_M and w (see Fig. 7); the addition of the Planck prior partially breaks this degeneracy, and the number of SNe in the highest redshift bin therefore decreases.

The case of evolving w is qualitatively similar, with one important difference: the high- z subsample of SNe is always present in the optimal distribution, regardless of the prior or the value of m . As Fig. 11 shows, the highest redshift bin always has a significant number of SNe ($\simeq 500$), even for $m = 6$, when their cost is large.

Although the exact optimal distribution for a given value of m , and the corresponding values of σ_w and σ_{w_1} , will depend in practice on details of the optimization — the number of redshift bins and the maximum number of SNe allowed per bin — some clear trends emerge from this analysis. While the lower redshift bins become relatively more populated in the optimal distributions (reflecting the lower cost of low-redshift SNe), the importance of high redshift supernovae remains: in *all* cases, at least 800 SNe are at redshifts $z > 1$. For the constant w case with no Planck prior, or for evolving w regardless of prior, these high-redshift SNe are crucial to making the error on w small enough to be useful.

Clearly we have just scratched the surface with regard to resource-limited optimization; to proceed further, one would need a much more quantitative description of the resources available and the systematics.

V. SUMMARY AND CONCLUSIONS

Unraveling the nature of dark energy is one of the outstanding challenges in physics and astronomy. Determining its properties is critical to understanding the Universe and its destiny and may shed light on the fundamental nature of the quantum vacuum and perhaps even of space-time. Type Ia supernovae and CMB anisotropy can both probe the dark energy equation-of-state w , and we have explored in detail the synergy between the two. With the MAP mission in progress, the Planck mission slated for launch in 2007, and the design of dedicated SN surveys now underway, such a study is very timely.

CMB anisotropy alone cannot tightly constrain the properties of dark energy because of a strong degeneracy between the average equation-of-state and the matter density. SNe can probe w with a precision that improves significantly with knowledge of the matter density, because $H_0 r(z)$ depends only upon w and Ω_M . A key result of this paper is that CMB anisotropy measurements by the upcoming Planck mission have even more potential for improving the ability of SNe to probe dark energy. The reason is simple: in the Ω_M - w plane (Fig. 1), the CMB constraint is more complementary to the SNe constraint than is determination of Ω_M .

Compared to the matter density prior $\sigma_{\Omega_M} = 0.03$, Planck CMB data reduce the predicted error σ_w (under the assumption of constant w) by about a factor of

two (Fig. 7). In probing possible variation of w with redshift, the Planck prior is also significantly better than the same matter density prior (Fig. 9). Given the concern expressed by some (e.g., [25]) that a precise measurement of the matter density independent of dark energy properties may be difficult, this is good news. On the other hand, we find that even if MAP can successfully measure polarization on large scales, its potential for complementarity with SNe falls short of that for Planck and is not as good as the $\sigma_{\Omega_M} = 0.03$ matter density prior.

We have also explored how the SNe determination of the dark energy equation-of-state, with or without prior information from the CMB or the matter density, depends upon the redshift distribution of the survey, including the effects of systematic error and a realistic spread of SNe redshifts. For either constant or evolving w , the optimal strategy calls for significant numbers of SNe above redshift $z \sim 1$. For the constant w case with no Planck prior, or for evolving w regardless of prior, these high-redshift SNe are necessary for achieving $\sigma_w < 0.1$. Observing substantial numbers of SNe at these high redshifts also provides the only hope of probing time evolution of the equation-of-state with reasonable precision. Moreover, the improvement in $\sigma_{dw/dz}$ continues to high redshift: $\sigma_{dw/dz}$ falls by more than a factor of two when z_{\max} increases from 1 to 2 (Fig. 9). Since we currently have no prior information about (or consensus physical models which significantly constrain) the time variation of w , the design of a SNe survey aimed at probing dark energy should take into account the possibility that w evolves. These conclusions about the need for high-redshift supernovae do not change significantly if we consider a hypothetical survey for which resources are constrained and a redshift-dependent cost is assigned to each supernova.

Ref. [11] raised the question whether a shallow SNe survey is better than a deep one in determining the dark energy equation-of-state, given prior knowledge from the CMB. Our results indicate that it is not, once the SNe and CMB experiments are realistically modelled. On the contrary, CMB/SNe complementarity strengthens the case for a deep SNe survey that extends to redshift $z \sim 2$.

ACKNOWLEDGMENTS

This work was supported by the DoE (at Chicago, Fermilab, LBL, and CWRU), NASA (at Fermilab by grant NAG 5-7092), and the NSF Center for Cosmological Physics at Chicago. EL would like to thank Ramon Miquel and Nick Mostek for their help with computations. DH thanks Wayne Hu for conversations regarding the MAP and Planck CMB missions.

REFERENCES

[1] S. Perlmutter et al, *Astrophys. J.* **517**, 565 (1999)

[2] A. Riess et al, *Astron. J.* **116**, 1009 (1998)
 [3] See, e.g., M.S. Turner, *Astrophys. J.*, in press (astro-ph/0106035); A. Lewis and S. Bridle, astro-ph/0205436
 [4] M.S. Turner and M. White, *Phys. Rev. D*, **56**, R4439 (1997)
 [5] S. Perlmutter, M.S. Turner and M. White, *Phys. Rev. Lett.* **83**, 670 (1999)
 [6] See, e.g., S. Weinberg, *Rev. Mod. Phys.* **61**, 1 (1989)
 [7] See, e.g., A. Dolgov, in *The Very Early Universe*, eds. G.W. Gibbons, S.W. Hawking, and S. Siklos (Cambridge University Press, 1983); K. Freese, F. Adams, J. Frieman, and E. Mottola, *Nucl. Phys. B* **287**, 797 (1987); B. Ratra and P.J.E. Peebles, *Phys. Rev. D* **37**, 3406 (1988); C. Wetterich, *Nucl. Phys. B* **302**, 668 (1988); J. Frieman et al, *Phys. Rev. Lett.* **75**, 2077 (1995); R.R. Caldwell, R. Dave, and P.J. Steinhardt, *Phys. Rev. Lett.* **80**, 1582 (1998); M. Bucher and D.N. Spergel, *Phys. Rev. D* **60**, 043505 (1999); for a review, see S.M. Carroll, astro-ph/0107571
 [8] K. Coble, S. Dodelson, and J. Frieman, *Phys. Rev. D* **55**, 1851 (1996); R. Dave, R.R. Caldwell, and P.J. Steinhardt, astro-ph/0206372
 [9] C.T. Hill and G. Ross, *Nuc. Phys. B* **311**, 253 (1988); S.M. Carroll, *Phys. Rev. Lett.* **81**, 3067 (1998)
 [10] D. Huterer and M.S. Turner, *Phys. Rev. D* **64**, 123527 (2001)
 [11] D.N. Spergel and G.D. Starkman, astro-ph/0204089, v2
 [12] See, e.g., E.V. Linder, astro-ph/0208xxx
 [13] M. Tegmark, astro-ph/0101354
 [14] W. Hu and N. Sugiyama, *Astrophys. J.* **444**, 489 (1995)
 [15] Planck: <http://astro.estec.esa.nl/SA-general/Projects/Planck>
 [16] D. Eisenstein, W. Hu, and M. Tegmark, *Astrophys. J.* **518**, 2 (1999)
 [17] W. Hu et al, *Phys. Rev. D.* **59**, 023512 (1998)
 [18] MAP: <http://map.gsfc.nasa.gov>
 [19] SNAP: <http://snap.lbl.gov>
 [20] M.M. Phillips, *Astrophys. J. Lett.* **413**, L105 (1993)
 [21] Nearby Supernova Factory: <http://snfactory.lbl.gov>
 [22] W. Freedman et al., *Astrophys. J.* **553**, 47 (2001)
 [23] S. Basa et al., in *Resource Book on Dark Energy* (Yellow Book), Community memos for the Snowmass 2001 Workshop on the Future of Particle Physics, ed. E. Linder, <http://supernova.lbl.gov/~evlinder/sci.html>
 [24] E.V. Linder and D. Huterer, astro-ph/0208yyy
 [25] I. Maor, R. Brustein, and P. J. Steinhardt, *Phys. Rev. Lett.* **86**, 6 (2001)